EUROGRAPHICS 2018 / D. Gutierrez and A. Sheffer
(Guest Editors)

Volume 37 (2018), Number 2

Controllable Dendritic Crystal Simulation Using Orientation Field

Bo Ren[1] and Jiahui Huang[2] and Ming C. Lin[3] and Shi-Min Hu[2,4]

[1]College of Computer and Control Engineering, Nankai University, Tianjin, China
[2]Department of Computer Science and Technology, Tsinghua University, Beijing, China
[3]Department of Computer Science, UNC Chapel Hill, USA
[4]School of Computer Science and Informatics, Cardiff University, UK

Abstract

Real world dendritic growths show charming structures by their exquisite balance between the symmetry and randomness in the crystal formation. Other than the variety in the natural crystals, richer visual appearance of crystals can benefit from artificially controlling of the crystal growth on its growing directions and shapes. In this paper, by introducing one extra dimension of freedom, i.e. the orientation field, into the simulation, we propose an efficient algorithm for dendritic crystal simulation that is able to reproduce arbitrary symmetry patterns with different levels of asymmetry breaking effect on general grids or meshes, including spreading on curved surfaces and growth in 3D. Flexible artistic control is also enabled in a unified manner by exploiting and guiding the orientation field in the visual simulation. We show the effectiveness of our approach by various demonstrations of simulation results.

CCS Concepts

•***Computing methodologies*** → ***Physical simulation;***

1. Introduction

The natural beauty of crystals has attracted much attention of artists and scientists for decades. One of the most charming patterns of crystals is dendritic crystal. Often formed when temperature falls below freezing point or in already supercooled liquids, it can be commonly observed in snowflake formations and frost patterns on the window. It is also one of the most common forms of solidifying composites, metals and alloys, such as in electrolytically refined metal crystals and mineral stones. There is a wide variation in the visual appearances of dendrites, while perfectly symmetrically structured shapes, such as hexagonal snowflakes exists, certain extent of disorder, or symmetry breaking, is widely observable in real-world dendritic crystals, leading to semi-structured self-organized shapes, e.g. feather-like pattern, eye-shaped structure and spherulite, etc. It is often the case that the natural beauty of dendrites inherits from the exquisite balance between structures of symmetry and asymmetry in the crystal formations.

On the other hand, in graphics applications, the crystal simulation can even go beyond reproducing natural shapes. Similar to guided simulation in gas and liquids, there is also potential for dendritic crystal simulation to form artistically directed shapes while preserving the intrinsic symmetric patterns. However, although it stands as an important part of solid-liquid phase transition and is commonly observable in daily life – either in scientific and industrious environments, little research has been devoted to the natural formation of dendritic crystals or the artistic control of such growth. Meanwhile, the existing works can only reproduce a limited subset of real-life dendrite patterns, or they do not provide enough freedom for adjusting symmetry breaking, variable symmetric patterns on arbitrary grids and meshes, or there is little to no artistic control of dendrite growth. These challenges remains in current literature.

In this paper, we present an extended non-isothermal dendritic crystal growth model that is not only capable of capturing a wide range of real-world dendritic crystal patterns, but can also provide flexible artistic control for simulations on mesh surfaces. Observing that ordered orientations appear in solid crystal molecules but not in liquids, dendritic crystallization is highly relevant to the changing process of orientations from disorder to order. In our approach, the conventional phase field equations for dendritic crystallization is enhanced by introducing one more variable in calculating the evolution of solid and liquid molecular orientation direction. We also provide a unified 3D dendrite simulation strategy in line with conventional 2D framework. By introducing orientation fields, controllable symmetry-breaking patterns can be reproduced on arbitrary 2D and 3D grids or meshes. The introduction of orientation fields also provides easy, intuitive artistic control to the dendrite shape. Our main contributions include:

- Physically-based dendritic crystallization method capable of capturing a wide range of real-world crystal shapes with an added dimension of local orientation calculation.
- Dendrite growth model reproducing arbitrary symmetry patterns in 2D and 3D on standard grids or 3D meshes, with controllable

symmetry breaking patterns that allow more diverse and richer appearance.
- Flexible and stable algorithmic framework, enabling direct artistic control to visual simulation.

2. Previous Works

Graphics research over the solidification process of liquid into solid dates back to [KG93], which proposes an physically-based icicle growth model. A random-walk strategy is adopted in their work to model the probabilistic freezing of water drops on the ice surface. Icicle formation is investigated again in [KAL06], where the liquid water freezing process is resolved by solving the thin-film Stefan problem. Later, ice freezing simulation is enhanced with contained air bubbles in [MTSK09, NIDN12, MX15], where water is assumed to bring dissolved air that forms bubbles during the freezing process. In these works, structured crystal patterns are not involved in the study.

In computer graphics, 2D structural dendritic crystallization has been studied by [KL03, KHL04]. A physical ice crystal growth model is proposed in [KL03] able to capture growth of ice dendrites, but their model confines to either perfect symmetry or isotropic patterns in 2D. A diffusion limited aggregation (DLA) model is further integrated in [KHL04] providing more realistic symmetry breaking appearance of ice crystal formation on surfaces. However, this hybrid approach in turn suffers from grid-dependent artifacts; the growth direction tends to follow the grid alignment. This algorithm is on hexagonal grids for water crystal simulation and the ability to simulate variable symmetric patterns on arbitrary grids or meshes is largely limited to DLA-based symmetry-breaking mechanics. Post-process bump/crease generation strategies are provided to enhance the rendering effect of the ice crystal shape, though no direct artistic control on the crystal growth is given. In our approach, by introducing a fast, local orientation calculation, we show how arbitrary growth patterns and variable randomness can be simultaneously achieved. The introduction of local orientation also enables direct artistic control and further enhancement of crystal rendering.

The dendritic crystallization problem has long received much attention in computational physics and crystal growth areas, with variants of phase-field based methods among the most effective models to reproduce real-world dendrite patterns. [Kob93] proposes a phase-field crystallization model that successfully generates dendrite patterns in single-component melt growth.

In [GBP02a, GBP02b, GPW*03, GPW04], isothermal models using orientation field are derived for 2D dendrite formation in alloy solutions, where concentration dynamics have to be modeled. Using axis-aligned assumption or small-angle approximation, [GW02, HhZfN08, PBG05] study octahedral growth in 3D. We take advantage of the orientation concept from [GBP02a, GBP02b] and integrate it into visual simulation of existing graphics non-isothermal framework saving the concentration calculation. The enhanced graphical model is capable of recovering dendrite shapes generated by the isothermal crystal growth models; it covers non-solution crystallization such as ice formation, and it also provides a precise strategy for arbitrary 3D orientation calculation free from approximations in previous methods, handling 2D and 3D simulations in a unified framework.

Our method has connections to graphics direction field designing and geometry synthesis works, where designing and analysis of rotational symmetric functions in 2D and 3D are studied. N-fold symmetric direction field designing on 2D manifolds are studied in [PZ07, RVAL09], where anisotropy is later considered in [DVPSH14]. In [HTWB11], 3D cubic-symmetric field is represented by the fourth band of spherical harmonics. However the above works do not cover all symmetry patterns for 3D anisotropy functions existing in dendritic crystallization model. We provide straightforward recipes to formulate most typical symmetry patterns in our approach. In addition, a geodesic polar map is used to represent relative location of nearby vertices on a triangle mesh in [LBZ*11], which is connected to the molecular orientation field calculation in 3D in our algorithm. An extensive survey for further reading on these research areas can be found in [VCD*16].

The dendritic crystal growth phenomenon is also linked to procedural modeling to some extent, where a large variety of tree models, urban districts are reconstructed from a simple set of generation rules and parameters, sharing a similarity with dendrite simulation [SPK*14, KFWM17, STBB14]. Structural models are also studied by example-based approaches such as in [ROM*15]. By using physically-based growth mechanisms, our approach reproduces real-world structured crystal shapes as well as provide flexible artistic control in the simulation.

3. Theoretical Foundations of Controllable Dendrite Growth

In this section we first briefly review the phase field theory for crystal growth in [Kob93, KL03, KHL04], i.e. the Kobayashi formulation adopted by previous works. Then, we introduce our extended model with support of local molecular orientation calculation.

3.1. Kobayashi Formulation Using Phase-Field Theory

The phase field theory for dynamics of crystallization is described by the evolution of a continuous phase-field value $\eta \in [0,1]$, with $\eta = 0$ indicating pure liquid phase and $\eta = 1$ indicating pure solid phase. A free energy is linked to each phase state, and the system evolves toward minimizing the free energy. Then the minimum points of free energy function correspond to steady states of the physical system, and governing equations can be derived from the free energy function using variational approach. For non-isotropic dendrite growth, since the steady state should be pure solid phase or pure liquid phase, the free energy function should have a double-well form, i.e. having exactly two local minima at $\eta = 0$ and $\eta = 1$. Temperature should affect the relative magnitude relation of the minima, making the global minimum position at $\eta = 1$ below freezing point and at $\eta = 0$ above it, in order that the system tends to settle at solid state below freezing point and vice versa. The free energy should also be higher in the phase front ($|\nabla\eta| > 0$) region to encourage phase transition there and discourage mixed state. In [Kob93], the free energy is given by

$$F(\eta,\xi) = \int \frac{1}{2}\varepsilon^2|\nabla\eta|^2 + f(\eta,\xi(T))d\mathbf{r} \tag{1}$$

In the above equation, $\xi(T) = \frac{\alpha}{\pi}arctan(\gamma(T_e - T))$ links the potential function f and the free energy function F with the temperature T, where T_e is equilibrium temperature and $\alpha \in (0,1)$ is a constant.

The anisotropy function ε is given as:

$$\varepsilon(\theta) = \bar{\varepsilon}(1 + \delta cos(j(\theta_0 - \theta))) \tag{2}$$

where $\bar{\varepsilon}, \delta$ are constants that affect the strength and peak-sharpness of the anisotropy function. The local phase front direction θ is linked to the phase field value η by $\theta = -\nabla\eta = -arccos[(\partial\eta/\partial x)/|\nabla\eta|]$ and θ_0 is a constant representing initial solid orientation. The equation for phase-field evolution is then derived by variational approach from Eqn.(1):

$$\frac{\partial\eta}{\partial t} = M_\eta(\nabla \cdot \frac{\partial F}{\partial \nabla\eta} - \frac{\partial F}{\partial \eta}) \tag{3}$$

where M_η is constant phase mobility coefficient that describes how easily the phase field changes. In [Kob93], after substituting Eqn.(1) into Eqn.(3), the equation for η has the form of:

$$\begin{aligned}\frac{\partial\eta}{\partial t} = M_\eta(\nabla \cdot (\varepsilon^2\nabla\eta) - \frac{\partial}{\partial x}(\varepsilon\frac{\partial\varepsilon}{\partial\theta}\frac{\partial\eta}{\partial y}) + \frac{\partial}{\partial y}(\varepsilon\frac{\partial\varepsilon}{\partial\theta}\frac{\partial\eta}{\partial x}) \\ +\eta(1-\eta)(\eta - \frac{1}{2} + \xi(T)))\end{aligned} \tag{4}$$

The last term comes from their choice of double-well function $f(\eta, \xi)$ which we will discuss in more detail later. The evolvement of temperature is governed by:

$$\frac{\partial T}{\partial t} = a^2\nabla^2 T + K\frac{\partial\eta}{\partial t} \tag{5}$$

where a^2 is heat diffusion coefficient and K is a latent heat constant. A higher K value leads to slower growth but with more branching effects in the final results.

The above phase field method is an effective model in simulating dendrite crystals, as is demonstrated in [KL03]. However it can only reproduce dendrites with little or no symmetry breaking other than complete isotropic growth. [KHL04] targets at this problem by integrating the DLA method into the simulation and successfully reproduces some extent of symmetry breaking effect, but they in turn suffer from grid-dependent artifacts where growth direction largely align with the grid formation, limiting ability of arbitrary growth other than ice crystallization on a hexagonal grid. By including calculation on the local molecular orientation, we introduce a more powerful simulation scheme.

3.2. Evolution of Local Orientation

The structure of dendrites is a result of microscopic ordering of molecular orientations in the solid phase. During the solidification process, unordered liquid molecules eventually settle into the same orientations as the nearby solid molecules. If this match of orientations is always perfect, the resulting dendrite will also be perfectly symmetric. Symmetry breaking happens when solidification proceeds too fast for complete orientation alignment, as the misoriented molecules will in turn influence newly solidifying ones and possibly change the growth direction.

Based on the above observation, it is natural to introduce a new degree of freedom into the phase field model that deals with aligning of molecular orientations in the simulation. Inspired by isothermal alloy dendrite growth models [GBP02a, GBP02b], we integrate a new equation calculating local molecular orientation changes during the solidification process into the Kobayashi model described in §3.1.

From an energy-based perspective, the reason behind the aligning tendency during dendritic crystallization is that misalignment between nearby molecules in solid crystals will result in higher free energy, while misalignment between liquid molecules cast little or no influence to the free energy. For clarity, we first write the free energy function in a more complete form than in Eqn.(1):

$$\begin{aligned}F = \int \frac{1}{2}\varepsilon^2|\nabla\eta|^2 + g(\eta) + p(\eta)(f_s(T) + f_{ori}(|\nabla\theta_{ori}|)) \\ +(1-p(\eta))f_l(T)d\mathbf{r}\end{aligned} \tag{6}$$

where $f_s(T)$ and $f_l(T)$ are temperature-dependent pure-solid-phase and pure-liquid-phase free energie densities,

$$f_{ori}(|\nabla\theta_{ori}|) = H|\nabla\theta_{ori}| \tag{7}$$

is misalignment energy density proportional to $|\nabla\theta_{ori}|$, absolute value of gradient of local molecular orientation θ_{ori}. Note θ_{ori} replaces θ_0 in Eqn.(2), and is now a variable. H is a constant coefficient. $g(\eta) = \frac{1}{4}\eta^2(\eta-1)^2$ from [GBP02a] ensures the free energy has a double-well form. $p(\eta)$ is an interpolation function on $[0,1]$. Comparing with the Kobayashi model, it is easy to verify that by dropping the $f_{ori}(|\nabla\theta_{ori}|)$ term and using $f_l = 0$, $f_s = -\frac{\xi(T)}{6}$ and $p(\eta) = \eta^2(3-2\eta)$, Eqn.(6) is simplified to Eqn.(1).

The phase field equation can be derived similarly by Eqn.(3):

$$\begin{aligned}\frac{\partial\eta}{\partial t} = M_\eta(\nabla \cdot (\varepsilon^2\nabla\eta) - \frac{\partial}{\partial x}(\varepsilon\frac{\partial\varepsilon}{\partial\theta}\frac{\partial\eta}{\partial y}) + \frac{\partial}{\partial y}(\varepsilon\frac{\partial\varepsilon}{\partial\theta}\frac{\partial\eta}{\partial x}) \\ -g'(\eta) - p'(\eta)(f_s - f_l + f_{ori}))\end{aligned} \tag{8}$$

Again this is similar to Eqn.(4) with the main difference being a newly introduced term f_{ori}.

An equation for θ_{ori} can be similarly derived using $\frac{\partial\theta_{ori}}{\partial t} = -M_{ori}(\nabla \cdot \frac{\partial F}{\partial\nabla\theta_{ori}} - \frac{\partial F}{\partial\theta_{ori}})$. From [GPW04], the second term is omittable, which gives:

$$\frac{\partial\theta_{ori}}{\partial t} = -M_{ori}H\nabla \cdot (p(\eta)\frac{\nabla\theta_{ori}}{|\nabla\theta_{ori}|}) \tag{9}$$

M_{ori} is a dimensionless orientational mobility and can be written as $M_{ori} = M_{ori,s} + (M_{ori,l} - M_{ori,s})(1-p(\eta))$, with $M_{ori,s}, M_{ori,l}$ representing the orientational mobility in pure solid and liquid phases. Assuming no mobility in pure solid, i.e. $M_{ori,s} = 0$, we drop the l,s footnote and re-write Eqn.(9) more explicitly as:

$$\frac{\partial\theta_{ori}}{\partial t} = -M_{ori}H(1-p(\eta))\nabla \cdot (p(\eta)\frac{\nabla\theta_{ori}}{|\nabla\theta_{ori}|}) \tag{10}$$

where M_{ori} is now a constant coefficient.

It is worth noting that from Eqn.(10), θ_{ori} does not change whether in pure liquid or pure solid phases since either $p(\eta)$ or $1-p(\eta)$ is 0 there. During the solidification, change in molecular orientation only happens within a layer at crystal growth front, which reflects exactly the physical behavior.

In our implementation we also choose $f_l = 0$, $f_s = -\frac{\xi(T)}{6}$ and $p(\eta) = \eta^2(3-2\eta)$ in the calculations, and Eqns.(5,8,10) serve as the fundamental equations of our model.

4. Enhanced Orientation-based Dendrite Growth Simulation

In this section we further investigate the potential of introducing orientation calculation. We also extend the orientation-based model to 3D.

4.1. Effect of Orientation Energy and the Orientation Equation

Intuitively the orientation energy density Eqn.(7) penalizes any neighborhood misorientation within regions where $\eta > 0$. As a result, according to Eqn.(10), liquid molecules tends to align with the solid crystal molecules until perfect alignment is achieved. Note the speed of this procedure is controlled by the orientation mobility coefficient M_{ori}. From a physical perspective, if M_{ori} is high enough or the crystallization process is slow enough, perfect symmetric dendritic crystals will form as all molecules align to each other. However, if M_{ori} is small compared to the phase transition rate, it will be possible that solidification is completed before perfect alignment is achieved, thus introducing symmetry-breaking patterns into the crystal structure. By adjusting the orientation mobility, we are able to introduce various levels of symmetry breaking effects, as is shown in Fig.1.

Eqn.(7) is capable of reproducing a set of real-world dendrite crystal growth. However, it still lack certain control on the final state of symmetry breaking. Taking the spherulite shown in the bottom line of Fig.5 as an example, while the branching direction is largely random on the local level, they also follow an obvious "bending" global pattern forming eye-shaped features in the dendrite.

For such more complex patterns a modified version of Eqn.(7) similar to that from [GPW04] can be used:

$$f_{ori} = \frac{H}{h}(xS_0 + (1-x)S_1) \tag{11}$$

$$S_0 = |sin(2\pi mh|\nabla\theta_{ori}|)|,\ h|\nabla\theta_{ori}| < \frac{3}{4m},\ otherwise\ 1 \tag{12}$$

$$S_1 = |sin(2\pi nh|\nabla\theta_{ori}|)|,\ h|\nabla\theta_{ori}| < \frac{1}{4n},\ otherwise\ 1 \tag{13}$$

where $x \in [0,1]$ is an interpolation factor. m,n are constants, h is grid width. The period of the sine function in S_1 is usually fixed to a large enough value so that it is monotonically increasing within the domain, while that in S_0 is smaller in order to form the shape of f_{ori} using the linear combination. Other than the zero point, the final shape of the f_{ori} curve has an extra local minimum with finite misorientation value, whose position can be controlled by adjusting m. Fig.3 shows f_{ori} shapes under different m and x values.

With orientation energy density f_{ori} in Eqn.(11), at the phase transition front, if a molecule has a smaller misorientation value, it can reduce the free energy by aligning itself to the solid crystal neighborhood. With larger misorientations, it will in turn settle to a branching direction corresponding to the minimum position of the f_{ori} curve.

Eqn.(11) can be directly inserted into Eqn.(8). Eqn.(10) needs to be slightly modified:

$$\frac{\partial\theta_{ori}}{\partial t} = -M_{ori}H(1-p(\eta))\nabla\cdot(2p(\eta)\pi(x\tilde{S}_0 m + (1-x)\tilde{S}_1 n)\frac{\nabla\theta_{ori}}{|\nabla\theta_{ori}|}) \tag{14}$$

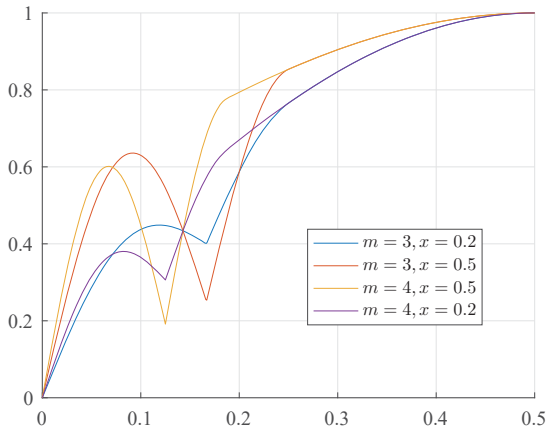

Figure 3: *f_{ori} curve in Eqn.(11) under different m and x values. The extra finite minima position is controlled by m.*

$$\tilde{S}_0 = sign[sin(2\pi mh|\nabla\theta_{ori}|)]cos(2\pi mh|\nabla\theta_{ori}|),\ h|\nabla\theta_{ori}| < \frac{3}{4m},\ otherwise\ 0 \tag{15}$$

$$\tilde{S}_1 = sign[sin(2\pi nh|\nabla\theta_{ori}|)]cos(2\pi nh|\nabla\theta_{ori}|),\ h|\nabla\theta_{ori}| < \frac{1}{4n},\ otherwise\ 0 \tag{16}$$

4.2. Three-Dimensional Dendritic Crystallization Model

Dendritic crystals show more complex and visually interesting shapes in three dimensional space, however previous works only provide limited access to 3D simulations of dendrite growth. By modifying the 3D orientation equation, we extend the above crystal growth model to three dimensions and provide precise formulations of 3D calculation with full support to various symmetry patterns.

Theoretically, in three dimensional space there are three rotational freedoms. However, in the simulation we rely on the phase field to recover the phase front direction which has only two rotational freedoms corresponding to the front normal direction. To avoid arbitrary calculation in self-rotation, we assume self-rotational angle is always zero. This simplification transforms the problem into two-dimensional space. Note that this is equivalent to assuming the mobility in self-rotational dimension to infinite, and can be justified by observing the real-world crystals, whose shapes seldom twist around its growth axis.

The local phase front direction θ and molecular orientation direction θ_{ori} are substituted with spatial directions $\Omega(\theta,\varphi) = -\nabla\eta$ and $\Omega_{ori}(\theta_{ori},\varphi_{ori})$. Using the phase field, we can define $\theta = -arccos((\partial\eta/\partial z)/|\nabla\eta|)$ and $\varphi = -arctan((\partial\eta/\partial y)/(\partial\eta/\partial x))$. The 3D phase equation corresponding to Eqn.(8) can then be derived by variational approach which gives:

$$\begin{aligned}\frac{\partial\eta}{\partial t} = M_\eta(\nabla\cdot(\varepsilon^2\nabla\eta) &+ \frac{\partial}{\partial x}(\frac{\varepsilon}{\tau}\frac{\partial\varepsilon}{\partial\theta}\frac{\partial\eta}{\partial x}\frac{\partial\eta}{\partial z} - \frac{\varepsilon}{\tau^2}\frac{\partial\varepsilon}{\partial\varphi}|\nabla\eta|^2\frac{\partial\eta}{\partial y}) \\ &+ \frac{\partial}{\partial y}(\frac{\varepsilon}{\tau}\frac{\partial\varepsilon}{\partial\theta}\frac{\partial\eta}{\partial z}\frac{\partial\eta}{\partial y} + \frac{\varepsilon}{\tau^2}\frac{\partial\varepsilon}{\partial\varphi}|\nabla\eta|^2\frac{\partial\eta}{\partial x}) \\ &- \frac{\partial}{\partial z}(\varepsilon\frac{\partial\varepsilon}{\partial\theta}\tau) - g'(\eta) - p'(\eta)(f_s - f_l + f_{ori}(||\nabla\Omega_{ori}||))\end{aligned} \tag{17}$$

Figure 1: *Comparison of symmetry breaking strategies. Top: Our result using orientation field. Different extent of symmetry breaking is achieved for a 5-fold pattern using large to small orientational mobilities (from left to right, M_{ori} is set to $30, 20, 15, 10, 5$). Middle: Adding noise to phase field from the previous model [Kob93, KL03]. From left to right, noise level is set to $5, 15, 25, 60, 100$. Broken linkage of phase field appears at relatively small randomness and eventually the result becomes no longer natural. Bottom: Alternatively using 'pin points' to randomly vary orientation direction instead of calculating Eqn.(10). Similar results with the top line is achieved with varying amount of random pin point numbers (from left to right: $0.1\%, 0.2\%, 1\%, 3\%, 10\%$ of total grid numbers).*

where $\tau = \sqrt{(\frac{\partial \eta}{\partial x})^2 + (\frac{\partial \eta}{\partial y})^2}$. The orientation equations Eqn.(10,14) remains exactly in the same form except θ_{ori} is substituted for Ω_{ori}, e.g. Eqn.(10) now turns into:

$$\frac{\partial \Omega_{ori}}{\partial t} = -M_{ori} H(1 - p(\eta)) \nabla \cdot (p(\eta) \frac{\nabla \Omega_{ori}}{||\nabla \Omega_{ori}||}) \qquad (18)$$

The algebraic operation of Ω_{ori} has to be defined in order to compute its gradient in 3D. Although Ω_{ori} can be represented by points ω on the unit sphere and parameterized by sphere coordinates (θ, φ) confined to the unit surface, such representation is inconvenient to define the "difference" between two orientation directions. Mathematically, the difference consists of two parts: one is the central angle calculated from the great circle distance between the two corresponding points on the unit sphere; the other is the direction of the great circle arc pointing from one point to the other. Due to the complex formula for calculating central angles in sphere coordinates, using (θ, φ) parameters in the differential equations, especially in the orientation equation, is exhaustive and unnecessary. We in turn derive a novel strategy that can compute the precise difference of Ω_{ori}. Specifically, at each ω position, all points on the unit sphere are represented in a designed local polar coordinates (ρ, λ) as follows. Given local coordinate axes at ω, a point on the unit sphere has its ρ value equal to the central angle it forms through great circle with ω; λ equals the angle value of that point after stereographic projection using the local coordinate at ω. Then any difference between two ω (or Ω_{ori}) can be represented by a (ρ, λ) pair in one of the ω's local polar coordinate. Note the (ρ, λ) pair is equivalent to a geodesic polar map [LBZ*11] of points on unit sphere with respect to ω.

Algorithm 1 Calculation of $\nabla \Omega_{ori}$

```
for each grid position p do
    Represent Ω_{ori,p} by point ω_p on the unit sphere
    Specify stereographic projection and polar coordinate at ω_p
    for each grid position q in p's neighborhood do
        Represent Ω_{ori,q} by point ω_q on the unit sphere
        Set ρ_q to central angle by great circle between ω_p, ω_q
        Project ω_q to ω̃_q by stereographic projection onto a plane
        Set λ_q to the angle value of ω̃_q in polar coordinate
    end for
    Calculate ∇Ω_ori at p as matrix product of ∇ and obtained
vector field (ρ, λ) in p's neighborhood.
end for
```

This approach enables explicit calculation of $\nabla \Omega_{ori}$ in 3D equations. Within calculation of the current grid, the Ω_{ori} values in neighborhood grids are transformed into local polar coordinate (ρ, λ) parameterization at the current-grid ω point from their (θ, φ)

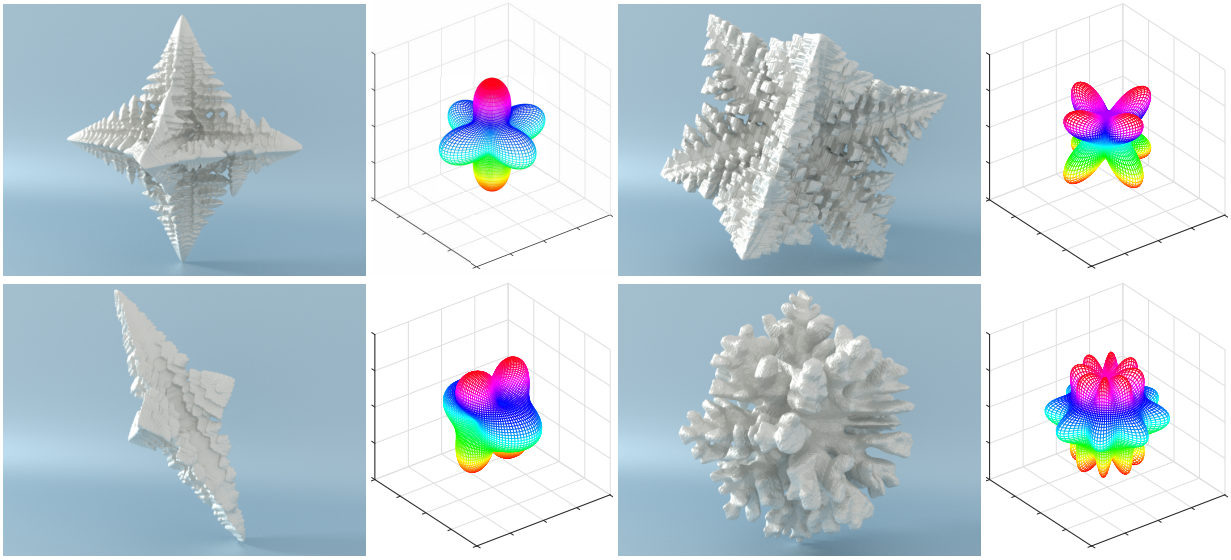

Figure 2: *3D dendrites of different symmetry patterns and their anisotropy function diagrams. Top: "perfect" patterns (octahedral and cubic). Bottom: "semi-perfect" patterns using Eqn.(26), with $a=3,b=2,l=1$ and $a=3,b=4,l=2$ separately.*

parameterizations. $\nabla\Omega_{ori}$ is then represented on this local coordinate as a 3×2 matrix, which is the product of the 3×1 operator ∇ and 1×2 vector field (ρ,λ). Then $||\nabla\Omega_{ori}||$ is calculated using the 2-norm of the matrix, which is needed for the computation of phase equation. A pseudo code for calculation of $\nabla\Omega_{ori}$ is given in Algorithm.4.2.

In our 3D simulation scheme, the orientation equation Eqn.(18) is calculated at each ω's local polar coordinate using the (ρ,λ) representation. Specifically, we first obtain $\frac{\partial\Omega_{ori}}{\partial t}$ as a $(\tilde{\rho},\tilde{\lambda})$ pair from the right hand side of the equation, then $\Omega_{ori,t+1}$ should correspond to the point $\Delta t(\tilde{\rho},\tilde{\lambda})$ in the local polar coordinate (since $\Omega_{ori,t}$ corresponds to (0,0)). Finally, $\Omega_{ori,t+1}$ is transformed back to the global (θ,φ) coordinate.

4.3. Three-dimensional Anisotropy Functions

The anisotropy function ε still needs to be extended to cope with full 3D simulations. Symmetry patterns in 3D links to the spherical symmetry groups. We derive anisotropy functions for typical symmetric formations of graphics interest and describe further designing methods in this part. A useful observation is that dendrite growth follows the maxima directions of the anisotropy functions. As will be summarized in §5.5, this helps in designing the anisotropy functions, e.g. we can put maxima on each symmetric axis and the resulting crystal will show the kind of symmetry.

In some "perfect" symmetric patterns the intersections of symmetry axes with the unit sphere evenly samples the surface domain, such as in the tetrahedral, octahedral or icosahedral classes. Basic octahedral symmetry has been studied in previous computational physics works [HhZfN08] with the anisotropy function given as:

$$\varepsilon_o(\mathbf{n}) = c_1 + c_2(sin^4\tilde{\theta}(sin^4\tilde{\varphi}+cos^4\tilde{\varphi})+cos^4\tilde{\theta}) \qquad (19)$$

It is not difficult to verify that the above equation degenerates into the 2D case to 4-fold symmetry represented by Eqn.(2) with properly chosen constant coefficients c_1,c_2. We use $\tilde{\theta}$ and $\tilde{\varphi}$ representing the parameterization of the phase front direction Ω in the spherical coordinate with orientation direction Ω_{ori} as equator, which will be discussed in detail later. $\mathbf{n}=\mathbf{n}(\tilde{\theta},\tilde{\varphi})$ is unit vector describing difference between phase front direction and crystal molecular orientation, which is also possible to be transformed into local Cartesian coordinates using $\mathbf{n}=(sin\tilde{\theta}cos\tilde{\varphi},sin\tilde{\theta}sin\tilde{\varphi},cos\tilde{\theta})$.

The tetrahedral symmetry pattern can be reproduced using

$$\varepsilon_t(\mathbf{n}) = (c_1 + c_2 cos\tilde{\theta}sin^2\tilde{\theta}cos2\tilde{\varphi})^2 \qquad (20)$$

The cubic symmetry pattern can be derived from Eqn.(20) with

$$\varepsilon_c(\mathbf{n}) = \frac{1}{2}(\varepsilon_t(\tilde{\theta},\tilde{\varphi})+\varepsilon_t(\pi-\tilde{\theta},\tilde{\varphi})) \qquad (21)$$

The $\tilde{\theta},\tilde{\varphi}$ values can not be simply calculated as $\theta-\theta_{ori},\varphi-\varphi_{ori}$, which does not ensure correct calculation in latitudinal differences when neither Ω,Ω_{ori} directions align with the equator. However the phase-field equation Eqn.(17) needs to calculate partial derivatives of the anisotropy function to θ and φ, so given Ω_{ori}, we need to analytically represent $\tilde{\theta},\tilde{\varphi}$ as functions $\tilde{\theta}(\theta,\varphi),\tilde{\varphi}(\theta,\varphi)$. This is done by transforming the parameterizations between the global coordinate and Ω_{ori}-equator spherical coordinate as follows.

The result of a direction vector counter-clockwisely rotated around a direction $\mathbf{k}$ by an angle Θ is given by the Rodrigue's rotation formula

$$\mathbf{n_{rot}} = \mathbf{Rn} = (I + sin\Theta\mathbf{K} + (1-cos\Theta)\mathbf{K}^2)\mathbf{n} \qquad (22)$$

where

$$\mathbf{K} = \begin{pmatrix} 0 & -k_z & k_y \\ k_z & 0 & -k_x \\ -k_y & k_x & 0 \end{pmatrix} \qquad (23)$$

Note that (θ,φ) can be represented by unit vector

$\mathbf{u} = (sin\theta cos\varphi, sin\theta sin\varphi, cos\theta)$ in the global Cartesian coordinate as well as $(\theta_{ori}, \varphi_{ori})$ by $\mathbf{u}_{ori} = (sin\theta_{ori}cos\varphi_{ori}, sin\theta_{ori}sin\varphi_{ori}, cos\theta_{ori})$. A matrix $\mathbf{R}$ defined by using $\mathbf{k} = \mathbf{u}_{ori} \times \mathbf{u}_0$ and $\Theta = \theta_{ori}$, where $\mathbf{u}_0 = (0,0,1)$ is the unit vector in global z direction, can transform $\mathbf{u}$ to a local Cartesian coordinate with $(\theta_{ori}, \varphi_{ori})$ as z direction, i.e. $\tilde{\mathbf{u}} = \mathbf{Ru} = (\tilde{x}(\theta,\varphi), \tilde{y}(\theta,\varphi), \tilde{z}(\theta,\varphi))$. Then $\tilde{\theta} = arccos\tilde{z}$ and $\tilde{\varphi} = arctan(\tilde{y}/\tilde{x})$ can be analytically calculated from (θ,φ) values. We can apply the chain rule to compute the derivatives:

$$\frac{\partial \varepsilon}{\partial \theta} = \frac{\partial \varepsilon}{\partial \tilde{\theta}}\frac{\partial \tilde{\theta}}{\partial \theta} + \frac{\partial \varepsilon}{\partial \tilde{\varphi}}\frac{\partial \tilde{\varphi}}{\partial \theta} \tag{24}$$

$$\frac{\partial \varepsilon}{\partial \varphi} = \frac{\partial \varepsilon}{\partial \tilde{\theta}}\frac{\partial \tilde{\theta}}{\partial \varphi} + \frac{\partial \varepsilon}{\partial \tilde{\varphi}}\frac{\partial \tilde{\varphi}}{\partial \varphi} \tag{25}$$

The Rodrigue's rotation formula also helps in changing the anisotropic function itself. For example, $\varepsilon(\mathbf{Rn})$ will define a rotated anisotropy function around a certain vector.

We can also design "semi-perfect" symmetry patterns corresponding to the dihedral symmetry class using

$$\varepsilon = 1 + csin^l(a\tilde{\theta})cos^l(b\tilde{\varphi}) \tag{26}$$

where c is constant coefficient and a, b are integer values, l can be 1 or 2. Various symmetry patterns generated using the above formulas are shown in Fig.2.

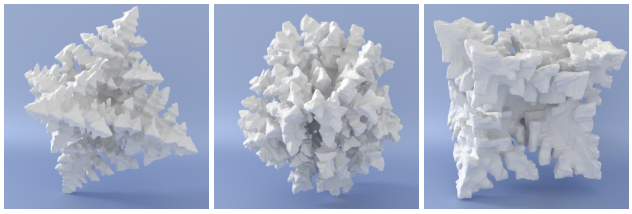

Figure 4: *3D dendrites with smaller orientational mobility setting in simulation. Left: octahedral with $M_{ori} = 60$; Middle: octahedral with $M_{ori} = 30$; Right: cubic with $M_{ori} = 50$.*

The above strategies give straightforward recipes to formulate most typical symmetry patterns. Note that spherical harmonics $y_l^m(\theta,\varphi)$ can help in the designation of anisotropic functions in 3D, e.g. the formulation of tetrahedral and cubic patterns can be linked to y_3^{-2} and y_3^2 bases. The base modes of the spherical harmonics further give a variety of symmetry functions, e.g. cubic-symmetric fields can be represented by the fourth band of spherical harmonics [HTWB11].

5. Implementation

In this section implementation issues are discussed. We address numerical problems raised for stable simulation and provide artistic control guidelines using the new orientation freedom. Following previous works [KL03, Kob93, GBP02a], the phase field equation and the orientation equation are solved explicitly. A convolutional method using Gaussian kernel described in [Bri08] is adopted for temperature equation to accelerate the computation. At the initial stage, the liquid phase is set to have random orientation values, and a solid phase seed is placed with a preset orientation value. A pseudo code of our algorithm framework is given in Algorithm.4.3.

Algorithm 2 Simulation Framework

```
Set initial random liquid orientation field
Set initial solid seeds and orientations
if useFixedGuideField then
    Set fixed orientation field value at given position
end if
while itr < itr_max do
    Solve phase field equation (Eqn.8, Eqn.17), store ∂η/∂t
    for all positions where orientation field is not fixed do
        Solve orientation equation (Eqn.10, Eqn.18)
    end for
    Solve Temperature equation (Eqn.5) using stored ∂η/∂t
    Output dendrite mesh from phase and orientation fields(§5.4)
end while
```

5.1. Numerical Issues in Solving the Governing Equations

We store the physical quantities in a staggered manner. We store the phase field and temperature field at the grid centers, and store the orientation field on grid edges. Standard staggered grid can be used for 2D and 3D simulations. The previous work [GPW04] reported that orientation equation must be solved at a time step $1/20$ of other equations. In our experiments with our staggered storage strategy time steps can be uniformed and the checker-board artifact originally appearing under higher time-step can be avoided.

Direct implementation of Eqn.(14) faces certain numerical instability since the function $x\tilde{S}_0 m + (1-x)\tilde{S}_1 n$ is discontinuous at the finite minimum of f_{ori} defined by Eqn.(11). This gives false estimation of the divergence if one directly calculates the difference between two neighboring storage positions when the $h|\nabla\theta|$ values of the two positions are on opposite sides of the discontinuity point. In this case we virtually create a "shrinked" grid inside the original grid centered at the current position, ensuring all points in the shrinked grid have $h|\nabla\theta|$ values on the same side of the discontinuity point. We interpolate the needed values on the shrinked grid from the original grid whenever necessary and compute the outermost divergence in Eqn.(14) on this virtual grid, giving a correct estimation.

Due to symmetry, when calculating difference between two directions, the result should be transformed into a congruent range modulo symmetry. For example, in a 4-fold symmetry in 2d, subtraction result between two direction angles should lie in the range $[-\frac{\pi}{4}, \frac{\pi}{4}]$. In 3D, semi-perfect cases from Eqn.(26) are handled similarly with θ, φ separately rounded. For perfect symmetry patterns, one can virtually place one of the two directions on a maximum direction of the anisotropy function and calculate the difference to be the difference from the other point to its nearest neighboring maximum.

5.2. Dendrite Growth on Arbitrarily Curved Surface

Axis-aligned growth models [KL03, KHL04, Kob93] are not straightforward to be applied to arbitrarily curved surfaces represented by general triangle meshes. On arbitrarily curved surfaces it is often impossible to find a consistent global coordinate system or a consistent parameterization mapping function especially when the triangle mesh is a closed surface. Since the anisotropic

functions are fixed on the direction of coordinates, dendrite growth directions cannot keep consistent on the whole curved surface but non-physically changes its direction according to local coordinate axes. Grid-dependent artifacts appearing in the simulation in previous work [KHL04] also prevent the extension to general triangle meshes of such methods.

Our approach does not fix growth direction with coordinate axes and define the anisotropy function based on difference between phase front direction and orientation direction. It avoids grid-dependent artifacts and enables application to arbitrarily represented surfaces by calculating consistent transformations of the orientation field between local coordinates of the vertices. On curved surfaces represented by triangle meshes, we adopt the affine technique from [RYL*17]. Specifically, the curved surface is locally flattened to a plane and the governing equations are evaluated on this plane within a 2d local coordinate. The phase front direction θ and orientation direction θ_{ori} fields are equivalently represented as 2d normalized direction vectors $\mathbf{n}$ and $\mathbf{n}_{ori}$ fields. They are stored within each vertex's local coordinate, and consistently transformed between local coordinates whenever needed using an affine matrix M_{ij} in [RYL*17]. Then differentials of variables can be calculated using a finite-volume based scheme on the triangle mesh. Such calculation does not require special mesh structure, so a standard triangle mesh can be used, and we store scalar and vector fields on mesh vertices as in [RYL*17].

5.3. Artistic Control of Growth Patterns

Our approach is able to control the extent of symmetry breaking effect by varying the orientation mobility, as is shown in §4.1 and Fig.1. In the simulation, higher mobility of orientation leads to more regular dendritic growth patterns, and vice versa.

The orientation field enables direct artistic control of crystal shapes. It is able to circumvent the calculation of orientation equation at certain "pin points" in the scene. This effectively means fixing the orientations of those points to controllable initial values. As a result the crystal growth direction will largely follow the fixed orientation directions when the phase front reaches those points. Initial values can also be set randomly to certain positions in the growth domain, providing an alternative way to generate symmetry breaking effect. Examples and more discussions will be given in §6.

It is also possible to map a wire-frame sketch into the simulation and initialize an orientation field in respect to it. For example, the random liquid orientation within a small band from the wire-frame can be initialized to have an average direction same to the tangential direction of the wire. This strategy enables directional growth following artistically designed draft shapes.

Furthermore, the form of Eqn.(10) can be exploited to simulate color variations along the crystal growth. That is, a "color field" C is defined and evolves using:

$$\frac{\partial C}{\partial t} = -M_C H(1-p(\eta))\nabla\cdot(p(\eta)\frac{\nabla C}{|\nabla C|}) \qquad (27)$$

which can be used in the rendering to generate chromatic appearance of the crystal.

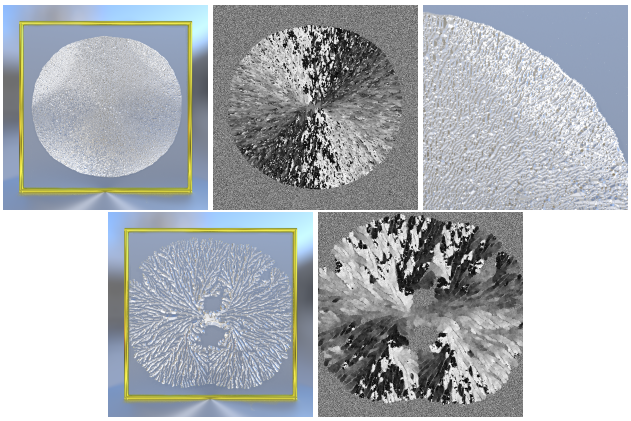

Figure 5: *Spherulites simulated using Eqn.(11). Top: from left to right shows the rendering result with recovered inner details from orientation field, orientation field, enlargement of the upper-right part. Bottom: from left to right shows the rendering result and orientation field. Radial veins structure and eye-shaped structure are reproduced. Figures can be enlarged for more details.*

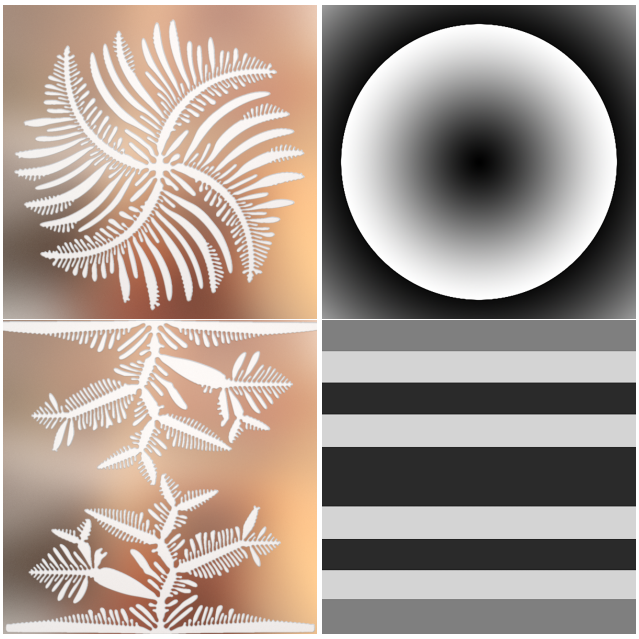

Figure 6: *Directly guided growth using our approach. On the right is color-mapped fixed orientation field guiding the dendrite growth.*

5.4. Post-processing of Dendrite Meshes

3D dendrite meshes can be recovered using marching-cube algorithm on the phase field. In 2D simulations, the phase field is flat, and creases and veins can be recovered following [KL03]. Then on 2D and curved surfaces, final dendrite mesh is generated from a height field as in [KL03,RYL*17]. Alternatively, for certain growth results where branches merge together forming a large solid plate of crystal region, we can recover the crystal detail from the orientation field. An intuitive motivation of the alternative approach is that regions of high orientation gradient are often the results of encounter of multiple separately-growing phase fronts. This means

solid phase there appears later and should be thinner if we assume the thickness growth is linear to time. On the other hand, from an energy-based perspective, the free energy is higher for solid phase in such region and will slow down the solidification process as well, which also makes the solid phase at such region appear later or even does not appear. This phenomenon can be observed both in real-world dendrites [GPW04] and in simulation results in §6. Thus after simulation, we can generate a height map from the orientation field. Specifically, we mask the output of θ_{ori} field with the phase field and consider solid-phase regions only. Then the canny edge detector [Can86] is used to find edges in the masked θ_{ori} field. The distance transform operator [RP68] is then applied on the solid-phase regions according to the edges. In this way, pixels far away from the edges in θ_{ori} field are assigned with larger height value and vice versa. Fig.5 shows an enhancement result to a spherulite dendrite, without the post-processing strategy using orientation field, there will be only a dull plain plate observable.

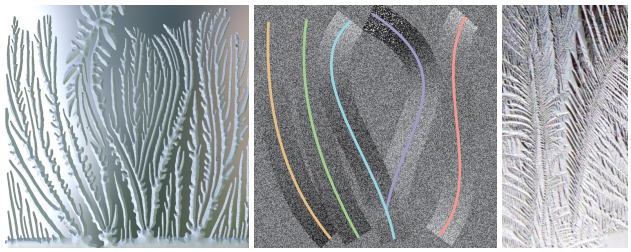

Figure 7: *Leaf-like ice crystal on a glass window. From left to right: rendered result; the initial field used in the simulation; leaf-like ice crystal photo from a winter window.*

Table 1: *Performance*

Case	Grid/Mesh Size	Avg. Time (msec/step)	Total Sim. Time (min)
Fig.1	512×512	2.1	0.13
Fig.2&4	$256 \times 256 \times 256$	121.9	2.1 ~ 16.8
Fig.5	1024×1024	8.1	1.0 ~ 1.7
Fig.6	1024×1024	5.1	1.1
Fig.7	1024×1024	8.0	3.0
Fig.8	$256 \times 256 \times 256$	105.4	1.8 ~ 8.8
Fig.9	2.62M vertices	63.4	15.9
Fig.10	7.49M vertices	214.4	35.7
Fig.11	$256 \times 256 \times 256$	110.8*	5.54*

* Average time for each dendrite.

5.5. Parameter Control in the Simulation

The final shape of the dendritic crystal simulated is influenced by a series of parameters K, M_{ori} and isotropy function choices. Here we give a brief description on their influences.

M_{ori} contributes to the symmetry breaking effect in all cases. Larger M_{ori} leads to less asymmetry keeping the ordered structure better. By using smaller M_{ori} in the simulation, asymmetry is stronger in the final crystal.

K has a large influence on the branching and growth speed of the phase field of crystals. Under larger K, the crystal generated will have more detailed branches, at a cost of slower growth speed and longer total simulation time. We typically use K between 1.5 and 1.8 for 2D simulation and 3 for 3D simulation.

The anisotropy functions $\varepsilon(\mathbf{n})$ control the symmetry patterns of the crystal shapes. Generally, the local growing direction as well as the final crystal shape will follow the $\mathbf{n}$ directions where $\varepsilon(\mathbf{n})$ reaches maxima. Sharper maxima peaks will generate thinner branches and leave more empty spaces between them in the final shape. These properties are helpful in designing symmetry patterns as well as rotating the symmetry axes to arbitrary directions using the Rodrigue's rotation formula.

6. Results

In this section we show various dendritic crystal growth results based on the orientation field calculation. We use time steps around 2×10^{-4}s in our simulation. We parallelize the calculation on a GeForce GTX 1080 Ti GPU. Detailed performances of the simulations are reported in Table.1. The total runtime reported are the running time from a single starting seed point to the full-growth shape at the end of simulation. Playback speed of the sequences in the supplemental video are adjusted to normalize the sequence lengths.

Fig.1 shows the influence of orientation field on symmetry breaking patterns on dendritic crystal growth. We compare our results on a 5-fold-symmetry dendrite with previous strategy given in [Kob93], whose method is adopted in [KL03], that adds random noise to the phase field. The top line shows our results and the middle line shows results using the method in [Kob93]. It is obvious that the previous strategy leads to broken and unnatural growth patterns due to direct modification of phase field using random noise, while our approach is able to naturally adjust the extent of symmetry breaking by changing the orientation mobility. In the bottom line the alternative way introduced in §5.3 is shown with a percentage of grids in the simulation domain fixed to random orientation initializations. In general, similar results to the top line is reproduced, however with this alternative strategy certain features appearing in real-world crystals, such as the "parallel arm" pattern in the $M_{ori} = 20$ result, are not observed in our experiments.

Fig.2 shows different 3D dendrites with their anisotropy functions. The top line contains the octahedral and cubic "perfect" symmetry patterns; the bottom line contains "semi-perfect" patterns using $a = 3, b = 2, l = 1, a = 3, b = 4, l = 2$ separately. Symmetry axis is rotated to be non-axis-aligned in some of the simulations, and in the cubic symmetry case we use $K = 3.5$. By decreasing the orientation mobility, more varied results are shown in Fig.4. It can be seen that our approach is able to recover visually interesting 3D dendrite shapes.

Fig.5 shows two types of real-world spherulite dendrite recovered using f_{ori} in Eqn.(11). The first one shows gradual bending of the branches during crystal formation into an eye-shaped structure. The second one isotropically expands the phase field during the simulation using $K = 0.8$, but with our alternative strategy described in §5.4 the inner structures can be reconstructed from the orientation field.

Fig.6 shows direct artistic guiding results using pin points. On

the top the simulation domain is set to fixed rotational orientation directions around the center seed point. On the bottom the simulation domain is divided by horizontal bands that each has a fixed orientation inside them. One can observe that controlled crystal growth by designed patterns can be generated using our approach.

Fig.7 uses user-defined curves to guide the growth direction of dendrites. Bezier curves are used to modify the initial random initial orientation fields. Within a small band beside the given curve orientation fields are biasedly randomized, i.e. their average direction is set to be the same with tangential direction of the curve. As a result leaf-like crystal shapes similar to ice frost on winter windows are created.

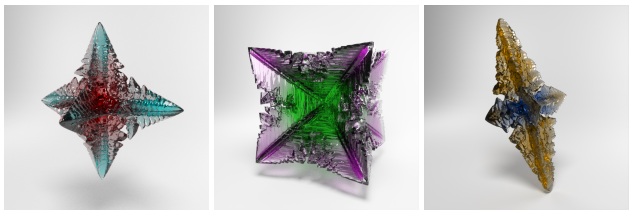

Figure 8: *Dendrite simulation with color field using Eqn.(27).*

Fig.8 shows color control results using Eqn.(27) in the 3D simulations. Polychromatic visual effect is achieved utilizing the color field obtained from the simulation by mapping the value to different colors.

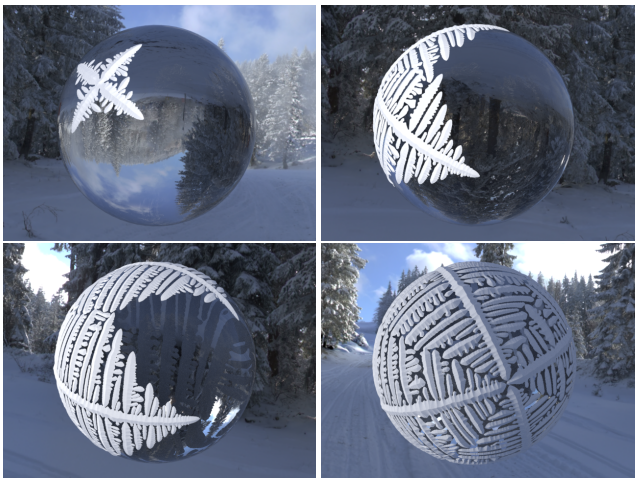

Figure 9: *Dendrite simulation on a ball using triangle mesh. The four branches meet at the other end of diameter.*

Fig.9 shows dendrite growth on curved triangle mesh. A 4-fold symmetric dendrite is simulated on a ball mesh. Growing on the surface without global coordinate, the four branches meet at the other end of diameter of the ball.

In Fig.10, frosty ice climbs across the human head from several seeds. We set higher temperature for some regions such as the eyes to suppress crystal growth in those places. As a result the crystals automatically climb around these regions.

In Fig.11 various 3D dendrites are formed as "crystal flowers". We use different perfect and semi-perfect symmetry patterns to generate a set of varied flower shapes on the tree model.

Figure 10: *Frosty ice climbs across the human head. Certain regions such as the eyes are set to have higher temperature, letting crystals grow around them.*

Figure 11: *Crystal flowers. Different perfect and semi-perfect symmetry patterns are used to generate a set of varied flower shapes on the tree model.*

7. Conclusion and Future Work

We have proposed an orientation-based dendritic crystal simulation method in this paper. The added freedom of orientation calculation in the physical model captures a wide range of real-world crystal shapes. Our approach reproduces realistic symmetry breaking effects in crystal patterns, while avoiding grid-dependent artifact appearing in previous work [KHL04]. With proper handling of the orientation equation, practical 3D dendrite growth model is proposed for 3D crystal simulation. The orientation field also provides effective artistic control strategies for graphical applications, such as artistic design, scientific visualization or science education etc.

There are possible future research directions for more in-depth study of 3D crystal growth patterns. The simplification of transforming the 3D problem into two-dimensional space implies that no symmetry breaking happens in the self-rotational dimension of freedom and perfect alignment is always maintained in this dimension. As a result, our approach cannot generate artistic effect of helix-like dendrite shapes that twists around growth axis. Currently introducing more symmetry axes does not always lead to branching toward new maxima directions both due to resolution limits and merging of neighboring branches. Detail enhancing techniques may lead to more visually interesting results. Integrating designation methods of arbitrary spherical functions based on spherical harmonics such as those originally adopted in rendering ([RH01])

will also be useful in designation of more complex anisotropy functions. For crystal growth on curved surfaces, it would be worthwhile developing control mechanisms that allow growth directions following geometric features, such as creases or ridges on the models. Currently the computation cost is higher on curved surfaces due to more calculation needed to handle model geometry, and it will benefit from further acceleration techniques. We would also like to investigate physical growth mechanism of mineral crystals, whose shapes consist of orderly aligned facets, such as diamond or quartz crystals.

Acknowledgments

This work is supported by the National Key R&D Program of China(2017YFB1002701), Natural Science Foundation of China(61602265), and US National Science Foundation.

References

[Bri08] BRIDSON R.: *Fluid Simulation for Computer Graphics*. A K Peters/CRC Press, Sept. 2008. 7

[Can86] CANNY J.: A computational approach to edge detection. *IEEE Transactions on Pattern Analysis and Machine Intelligence PAMI-8*, 6 (Nov 1986), 679–698. 9

[DVPSH14] DIAMANTI O., VAXMAN A., PANOZZO D., SORKINE-HORNUNG O.: Designing n-polyvector fields with complex polynomials. *Comput. Graph. Forum 33*, 5 (Aug. 2014), 1–11. 2

[GBP02a] GRÁNÁSY L., BÖRZSÖNYI T., PUSZTAI T.: Nucleation and bulk crystallization in binary phase field theory. *Phys. Rev. Lett. 88* (May 2002), 206105. 2, 3, 7

[GBP02b] GRÃąNÃąSY L., BÃűRZSÃűNYI T., PUSZTAI T.: Crystal nucleation and growth in binary phase-field theory. *Journal of Crystal Growth 237* (2002), 1813 – 1817. The thirteenth international conference on Crystal Growth in conj unction with the eleventh international conference on Vapor Growth and Epitaxy. 2, 3

[GPW*03] GRÁNÁSY L., PUSZTAI T., WARREN J. A., DOUGLAS J. F., BÖRZSÖNYI T., FERREIRO V.: Growth of'dizzy dendrites' in a random field of foreign particles. *Nature Materials 2*, 2 (2003), 92. 2

[GPW04] GRÃąNÃąSY L., PUSZTAI T., WARREN J. A.: Modelling polycrystalline solidification using phase field theory. *Journal of Physics: Condensed Matter 16*, 41 (2004), R1205. 2, 3, 4, 7, 9

[GW02] GEORGE W. L., WARREN J. A.: A parallel 3d dendritic growth simulator using the phase-field method. *Journal of Computational Physics 177*, 2 (2002), 264 – 283. 2

[HhZfN08] HOU H., HUI ZHAO Y., FENG NIU X.: 3d anisotropy simulation of dendrites growth with phase field method. *Transactions of Nonferrous Metals Society of China 18* (2008), s223 – s228. 2, 6

[HTWB11] HUANG J., TONG Y., WEI H., BAO H.: Boundary aligned smooth 3d cross-frame field. In *Proceedings of the 2011 SIGGRAPH Asia Conference* (New York, NY, USA, 2011), SA '11, ACM, pp. 143:1–143:8. 2, 7

[KAL06] KIM T., ADALSTEINSSON D., LIN M. C.: Modeling ice dynamics as a thin-film stefan problem. In *Proceedings of the 2006 ACM SIGGRAPH/Eurographics Symposium on Computer Animation* (Aire-la-Ville, Switzerland, Switzerland, 2006), SCA '06, Eurographics Association, pp. 167–176. 2

[KFWM17] KELLY T., FEMIANI J., WONKA P., MITRA N. J.: Bigsur: Large-scale structured urban reconstruction. SIGGRAPH Asia 2017, ACM. 2

[KG93] KHARITONSKY D., GONCZAROWSKI J.: A physically based model for icicle growth. *The Visual Computer 10*, 2 (Feb 1993), 88–100. 2

[KHL04] KIM T., HENSON M., LIN M. C.: A hybrid algorithm for modeling ice formation. In *Proceedings of the 2004 ACM SIGGRAPH/Eurographics Symposium on Computer Animation* (Aire-la-Ville, Switzerland, Switzerland, 2004), SCA '04, Eurographics Association, pp. 305–314. 2, 3, 7, 8, 10

[KL03] KIM T., LIN M. C.: Visual simulation of ice crystal growth. In *Proceedings of the 2003 ACM SIGGRAPH/Eurographics Symposium on Computer Animation* (Aire-la-Ville, Switzerland, Switzerland, 2003), SCA '03, Eurographics Association, pp. 86–97. 2, 3, 5, 7, 8, 9

[Kob93] KOBAYASHI R.: Modeling and numerical simulations of dendritic crystal growth. *Physica D: Nonlinear Phenomena 63*, 3 (1993), 410 – 423. 2, 3, 5, 7, 9

[LBZ*11] LI Y., BAO F., ZHANG E., KOBAYASHI Y., WONKA P.: Geometry synthesis on surfaces using field-guided shape grammars. *IEEE Transactions on Visualization and Computer Graphics 17*, 2 (Feb. 2011), 231–243. 2, 5

[MTSK09] MADRAZO C., TSUCHIYA T., SAWANO H., KOYANAGI K.: Air bubbles in ice by simulating freezing phenomenon. 2

[MX15] MIAO Y., XIAO S.: Particle-based ice freezing simulation. In *Proceedings of the 14th ACM SIGGRAPH International Conference on Virtual Reality Continuum and Its Applications in Industry* (New York, NY, USA, 2015), VRCAI '15, ACM, pp. 17–22. 2

[NIDN12] NISHINO T., IWASAKI K., DOBASHI Y., NISHITA T.: Visual simulation of freezing ice with air bubbles. In *SIGGRAPH Asia 2012 Technical Briefs* (New York, NY, USA, 2012), SA '12, ACM, pp. 1:1–1:4. 2

[PBG05] PUSZTAI T., BORTEL G., GRÃąNÃąSY L.: Phase field theory of polycrystalline solidification in three dimensions. *EPL (Europhysics Letters) 71*, 1 (2005), 131. 2

[PZ07] PALACIOS J., ZHANG E.: Rotational symmetry field design on surfaces. In *ACM SIGGRAPH 2007 Papers* (New York, NY, USA, 2007), SIGGRAPH '07, ACM. 2

[RH01] RAMAMOORTHI R., HANRAHAN P.: An efficient representation for irradiance environment maps. In *Proceedings of the 28th Annual Conference on Computer Graphics and Interactive Techniques* (New York, NY, USA, 2001), SIGGRAPH '01, ACM, pp. 497–500. 10

[ROM*15] ROVERI R., ÖZTIRELI A. C., MARTIN S., SOLENTHALER B., GROSS M.: Example based repetitive structure synthesis. *Comput. Graph. Forum 34*, 5 (Aug. 2015), 39–52. 2

[RP68] ROSENFELD A., PFALTZ J.: Distance functions on digital pictures. *Pattern Recognition 1*, 1 (1968), 33 – 61. 9

[RVAL09] RAY N., VALLET B., ALONSO L., LEVY B.: Geometry-aware direction field processing. *ACM Trans. Graph. 29*, 1 (Dec. 2009), 1:1–1:11. 2

[RYL*17] REN B., YUAN T., LI C., XU K., HU S. M.: Real-time high-fidelity surface flow simulation. *IEEE Transactions on Visualization and Computer Graphics PP*, 99 (2017), 1–1. 8

[SPK*14] STAVA O., PIRK S., KRATT J., CHEN B., MECH R., DEUSSEN O., BENES B.: Inverse Procedural Modelling of Trees. *Computer Graphics Forum* (2014). 2

[STBB14] SMELIK R. M., TUTENEL T., BIDARRA R., BENES B.: A survey on procedural modelling for virtual worlds. *Computer Graphics Forum 33*, 6 (2014), 31–50. 2

[VCD*16] VAXMAN A., CAMPEN M., DIAMANTI O., BOMMES D., HILDEBRANDT K., BEN-CHEN M., PANOZZO D.: Directional field synthesis, design, and processing. In *SIGGRAPH ASIA 2016 Courses* (New York, NY, USA, 2016), SA '16, ACM, pp. 15:1–15:30. 2